CrystEngComm

CrystEngComm

PAPER

Zn₂SiO₄ urchin-like microspheres: controlled synthesis and application in lithium-ion batteries

Shaoyan Zhang,*[a] Lei Ren[a] and Shengjie Peng*[b]

Three-dimensional (3D) Zn₂SiO₄ urchin-like microspheres were successfully synthesized by a simple and facile hydrothermal method without using any surfactants or additives. The as-prepared microspheres were built by one-dimensional (1D) nanorods, which interconnected with each other through self-assembly. The reaction conditions influencing the morphologies of the products such as reaction times,
10 reaction temperatures, and pH values were systematically investigated. The stepwise self-assembly formation mechanism for the hierarchical urchin-like microspheres was proposed on the basis of a series of time-dependent experiments. As a demonstration of the functional properties of such 3D architecture, Zn₂SiO₄ was investigated as a new anode material for lithium-ion batteries (LIBs). It was found that the Zn₂SiO₄ urchin-like microspheres exhibited high discharge capacity and good cycle stability, indicating
15 promising anode candidates in LIBs. Such attractive lithium storage performance presented an alternative anode material for high-performance LIBs.

1. Introduction

Over the past several years, rational synthesis and assembly of one-dimensional (1D) or two-dimensional (2D) nanostructures
20 into three-dimensional (3D) ordered complex architectures have triggered a worldwide interest because of their unique chemical and physical properties, leading to a wide range of potential applications in nanodevices.[1–6] Recently, the 3D micro- and nanostructures have also drawn significant research interest in
25 lithium-ion batteries (LIBs), due to their unique hierarchical structures and excellent kinetics.[7–9] It has been documented that the nanoscale building blocks in the hierarchical nanostructures can provide large interfacial contact area and short Li⁺ transport distance, resulting in superior rate capabilities.[10,11] Moreover, the
30 ordered and stable hierarchical nanostructures can buffer the huge volume changes during the lithium insertion/extraction process and alleviate the pulverization of the electrode material, which is beneficial for improving the cycling stability.[12,13] Inspired by the superiority of the 3D hierarchical nanostructures, much work has
35 been carried out on the synthesis of various 3D hierarchical nanostructured materials and their electrochemical properties.[13–17]

Zn₂SiO₄, as one of the most important multifunctional materials, has attracted much attention because of its excellent physical and chemical properties in various fields such as
40 phosphor host, paints, electronic insulators, cathode ray tubes, fluorescent lamps, adsorbents in water treatment, and so forth.[18–20] As structures and morphologies of functionals materials can significantly influence their properties, 1D Zn₂SiO₄ nanostructures with various morphologies have been reported,
45 including nanowires,[21] rice-like nanostructures,[22] and nanorods.[23,24] Until recently, 3D straw-bundle-like Zn₂SiO₄ architectures have been obtained through thermal evaporation

technique.[25] As is known, the thermal evaporation method has several disadvantages such as high temperature, high cost and
50 tedious synthetic procedures, which may limit their large-scale applications. Hydrothermal method as a typical solution-based approach has been proven to be an effective and convenient process in preparing various inorganic materials with diverse controllable morphologies.[26–28] This environmentally acceptable
55 method becomes attractive for their merits, including easily controllable reaction conditions, relatively large scale, and the use of water as the reaction medium, thus it could be prospective for the fabrication of 3D Zn₂SiO₄ hierarchical architectrues in a low-cost and scalable way.

60 It is known that Zn₂SiO₄ and rare earth ions doped Zn₂SiO₄ phosphors possess high luminous efficiency and chemical stability; however, their electrochemical properties have been rarely investigated. Willemite Zn₂SiO₄ is a natural orthosilicate with a phenacite-like structure in which Zn-O tetrahedra and Si-O
65 tetrahedra share corners to form hollow 'tubes' parallel to [0001].[29,30] Such a channel structure will facilitate the insertion and extraction of Li⁺, making Zn₂SiO₄ have potential applications as potential active materials in LIBs. Although Zn₂SiO₄ with various morphologies has been prepared, few attempts have been
70 made so far to study the electrochemical lithium insertion/deinsertion property of these unique Zn₂SiO₄ micro- or nanostructures. Until Recently, we reported hydrothermal synthesis and electrochemical properties of Zn₂SiO₄ nanorods and mesorods,[31] which as far as we know, is the first report on the
75 electrochemical property of this material. The Zn₂SiO₄ nanorods with larger specific surface area exhibited higher electrochemical activity than Zn₂SiO₄ mesorods and bulk materials. Therefore, developing a facile, economic, and effective strategy to prepare

3D Zn_2SiO_4 architectures and then exploring its electrochemical performance toward lithium are of great importance to expand its applied range.

In this paper, Zn_2SiO_4 urchin-like microspheres have been
5 successfully prepared on a large scale via a simple hydrothermal route using amorphous nano silica as silicon source. The final morphologies of the products were dependent on the reaction conditions, such as the pH values, reaction temperatures, and reaction times. This simple synthetic route, which involved no
10 templates or surfactants, can offer great opportunities for the scale-up preparation of 3D Zn_2SiO_4 and Zn_2SiO_4-based nanostructures. Moreover, the electrochemical properties of this material as anode materials have been investigated in LIBs. The results showed that the 3D Zn_2SiO_4 microspheres exhibited high
15 capacity and good cycling reversibility, indicating promising anode candidates for LIBs.

2. Experimental

2.1 Material Synthesis

All chemicals were of analytical grade and used without further
20 purification. Amorphous silica nanoparticles were prepared by conventional Stöber method.[32] In a typical synthesis, $Zn(NO_3)_2 \cdot 6H_2O$ (4 mmol) was dissolved in deionized water (10 ml) and silica nanoparticles (2 mmol) was added into the $Zn(NO_3)_2$ solution under vigorous stirring. Then, NaOH solution
25 (6 mL, 2M) was added with magnetic stirring for 15 min to form a solution with pH of ca. 14. The mixture was sealed in a Teflon-lined autoclave (20 mL), heated to 220 °C and maintained at that temperature for 24 h. After the reaction, the autoclave was cooled to ambient temperature naturally. The final products were
30 collected by centrifugation, washed with deionized water and ethanol, and then vacuum dried at 60 °C for 12 h. Contrast experiments were carried out by adjusting the pH values of precursors to 5, 7, and 10 by controlling the amount of NaOH solution. As a comparision, bulk Zn_2SiO_4 sample was synthesized
35 by traditional solid-state reaction method by mixing ZnO and SiO_2 with a molar ratio of 2:1 followed by heat treatement at 1300 °C for 8 h in air atmosphere.

2.2 Characterization

The crystalline structures of the products were analyzed with an
40 X-ray diffractometer (XRD, Bruker, D8 ADVANCE) with $Cu_{K\alpha}$ radiation (λ=1.5418Å) at a scan rate of 2°/min over the range of 10–80°. The morphologies of the as-prepared products were characterized by field-emission scanning electron microscopy (FESEM, JEOL, JSM-6700F) and transmission electron
45 microscopy (TEM, JEOL 2100F).

2.3 Electrochemical Measurements

The working electrode was fabricated by compressing a mixture of the active material, acetylene black-ATB, and polytetrafluoroethylene (PTFE) in a weight ratio of active
50 material:ATB:PTFE=7:2:1. The electrode was dried at 80 °C for 1 h and cut into a disk (1.0 cm^2). The electrolyte solution was 1.0 M $LiPF_6$ dissolved in a mixture of ethylene carbonate (EC) and dimethyl carbonate (DMC) with a volume ratio of EC:DMC=1:1. The cell assembly was performed in an Ar-filled glovebox. The
55 galvanostatic method at a discharge–charge current density of 50

mA g^{-1} and between fixed potential limits (0.02–2.5V) was used to measure the electrochemical capacity and cycle stability of the electrodes at room temperature using a LAND-CT2001A instrument. The cyclic voltammetry (CV) experiment was carried
60 out at a scan range of 0.01–3.0V (vs Li^+/Li) and a scan rate of 0.2 mV s^{-1} using a Gamry Reference 600 potentiostat at room temperature. The impedance measurements were carried out under the open-circuit condition in the frequency range from 1×10^6 to 0.1 Hz.

65 ## 3. Results and discussion

The phase and structure of the products were examined by X-ray diffractometer (XRD). Figure 1 showed the XRD pattern of the urchin-like Zn_2SiO_4 microspheres obtained under pH of ca. 14 and 220 °C for 24 h. All of the reflections could be readily
70 indexed to pure phase of Zn_2SiO_4 with the rhombohedral structure [JCPDS Card No. 37-1485]. The major reflections at 2θ = 25.45°, 31.46°, and 33.96° corresponding to the (220), (113), and (410) planes, respectively, could be seen clearly. No other impurities were detected, indicating the high purity of the product
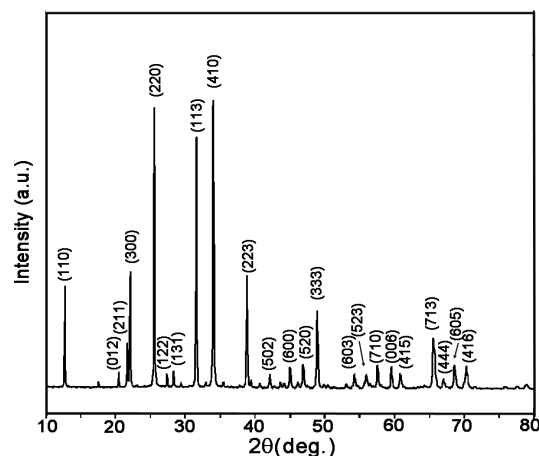75 and completed reaction during the process.

Fig. 1 XRD pattern of the as-prepared Zn_2SiO_4 urchin-like microspheres.

80 The morphologies of the as-prepared samples were investigated by field-emission scanning electron microscopy (FESEM), transmission electron microscopy (TEM) and high-resolution TEM (HRTEM). The overall FESEM image in Figure 2a demonstrated that the sample consisted of a large number of
85 microspheres with a narrow size distribution, which look like urchin (inset). The average size of the microspheres was about 8 μm. The as-prepared urchin-like microstructures could not be destroyed and broken into discrete individual nanorods even by subjecting their aqueous suspension to ultrasonication for 6 h,
90 indicating that the urchin-like microspheres were not constructed by random aggregated nanorods but in an oriented manner. More detailed FESEM images, as displayed in Figure 2b and 2c, showed that the urchin-like microsphere was composed of abundant nanorods with a diameter of ca. 100 nm and an aspect
95 ratio of ca. 40. The nanorods were self-assembled in a radial way to form the urchin-like microspheres. It was expected that this unique structure with high stability might have a high surface

area, which could provide high specific capacity due to the easy access of the active materials in the redox process to their interface. Figure 2d displayed a representative TEM image of an individual Zn_2SiO_4 microsphere. It was found that almost entire nanorods were assembled in a radial form from the center to the surface of spheres which looked like a sea urchin as a whole. From the HRTEM image in Figure 2e, it could be seen that the surface of the Zn_2SiO_4 nanorods was smooth. The selected-area electron diffraction (SAED) pattern revealed a spot pattern proving the single-crystal nature of the product. The clearly resolved lattice fringe in Figure 2f was calculated to be about 0.26 nm, corresponding to the (410) plane of rhombohedral structured Zn_2SiO_4.
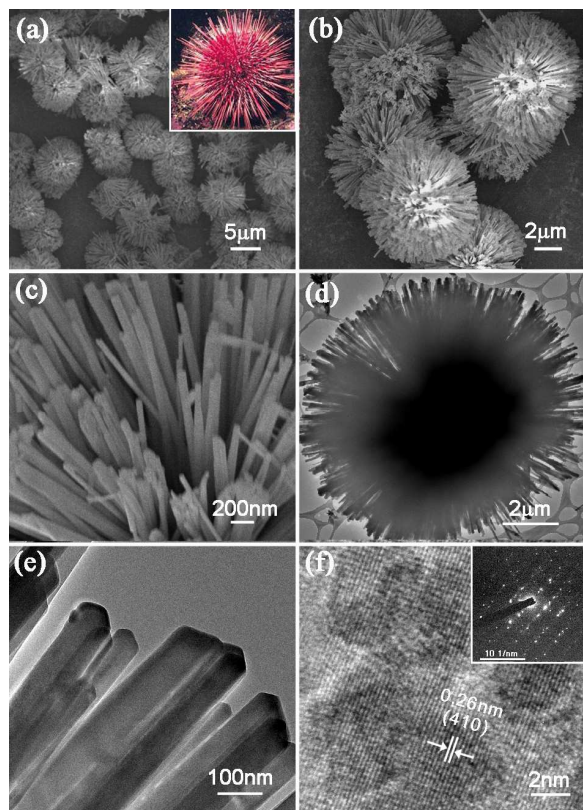

Fig. 2 (a)–(c) FESEM, (d), (e) TEM, and (f) HRTEM images of the as-prepared Zn_2SiO_4 urchin-like microspheres. The insets of Figure 2 (a) and (f) are the photo of an urchin and SAED pattern, respectively.

It was found that the pH values in the solution can influence the morphology of the products. Figure 3 showed the morphologies and corresponding XRD patterns of the products obtained at different pH values. When the pH value of the precursor suspension was adjusted to 5, the product consisted of well dispersed nanoparticles of a size of about 100 nm (Figure 3a). When adjusting to pH 7, all nanoparticles evolved to short nanorods with diameters of 80–100 nm (Figure 3b). Further increasing the pH of the precursor mixture resulted in a further increase in the lengths of the nanorods. When the pH was adjusted to 10, the length of the nanorods increased to about 600 nm (Figure 3c), and well-defined urchin-like microspheres with narrowly distributed diameters were finally obtained at the pH of

14. The XRD patterns of products obtained at various pH values could be identified as the pure and rhombohedral structure of Zn_2SiO_4 (Figure 3d). These results revealed that self-assembly process could occur at a high pH value, which was important for the formation of the urchin-like microspheres.
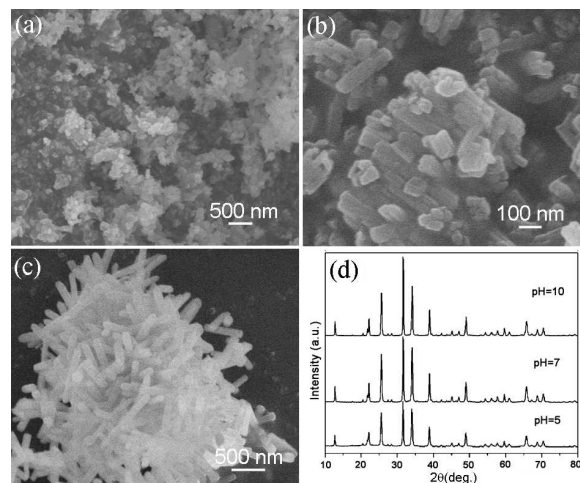

Fig. 3 (a)–(c) FESEM images and (d) XRD patterns of the products obtained at different pH value: (a) 5, (b) 7, and (c) 10.

To reveal the growth process of such interesting hierarchical urchin-like Zn_2SiO_4 microspheres, time-dependent experiments were carried out. Figure 4 and Figure 5 showed XRD patterns and FESEM images of the products obtained at 220 ºC for different reaction times. As shown in Figure 4, at the initial 1 h, all of the reflections could be indexed to a hexagonal phase of ZnO (JCPDS Card No. 36-1451) and no reflections of SiO_2 appeared, indicating that ZnO was formed at the early stage and the SiO_2 did not react with ZnO. The FESEM image (Figure 5a) showed this sample was mainly composed of 2D thin nanosheets and irregular nanoparticles. After the reaction for 3 h, the reflections of ZnO completely vanished, all of the reflections could be indexed to the pure phase of $Zn_4Si_2O_7(OH)_2 \cdot H_2O$ (JCPDS Card No. 05-555). The sample was composed of irregular bulk materials with typical sizes of about 1–2 μm (Figure 5b). When the reaction time was prolonged to 4.5 h, a new crystal phase, which could be ascribed to Zn_2SiO_4 (JCPDS Card No. 37-1485), began to coexist with $Zn_4Si_2O_7(OH)_2 \cdot H_2O$. The morphology of the sample was shown to be a coexistence of bulk materials, nanorods and lots of nanoparticles aggregates (Figure 5c). With the reaction processing (6 h), the intensitys of the reflections of Zn_2SiO_4 increased; while the reflections of $Zn_4Si_2O_7(OH)_2 \cdot H_2O$ were barely observed, indicating that $Zn_4Si_2O_7(OH)_2 \cdot H_2O$ was an intermediate phase in the reaction. The morphology of the product obtained at 6 h was shown to be a coexistence of nanorods and nanoparticles aggregates, and the bulk materials completely disappeared (Figure 5d). When the reaction time was prolonged to 10 h (Figure 5e), numerous nanorods were observed and the number of particles gradually decreased, suggesting that the longer nanorods grow at the expense of smaller particles. Interestingly, it was noticed that some nanorods attached with each other to form a straw-bundle-like architecture (inset). When the reaction time was increased to 14 h or longer, underdeveloped urchin-like microspheres were observed in the product as shown

in Figure 5f. Meanwhile, the relative intensity of the reflections for Zn_2SiO_4 increased gradually, suggesting an increase in the crystallite size with further increased reaction time.
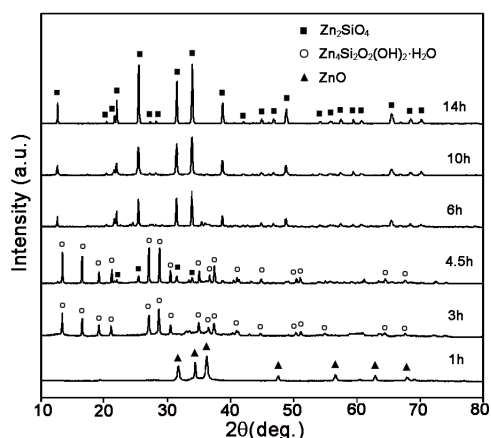

Fig. 4 XRD patterns of the products obtained at different hydrothermal reaction times (1 h, 3 h, 4.5 h, 6 h,10 h, and 14 h).
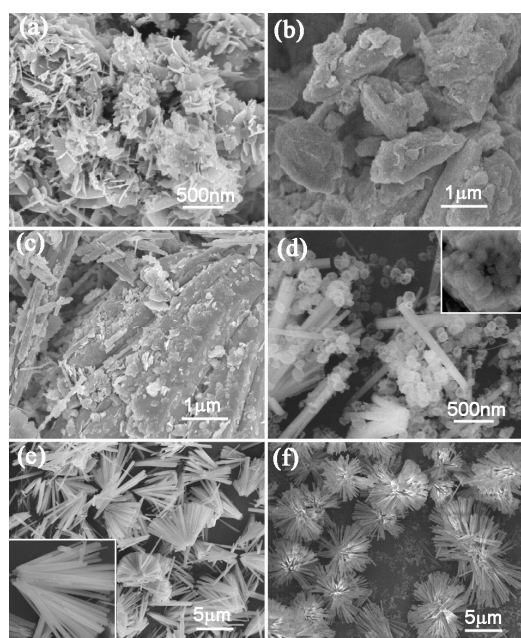

Fig. 5 FESEM images of the products obtained at different hydrothermal reaction times: (a) 1, (b) 3, (c) 4.5, (d) 6, (e) 10, and (f) 14 h.

In general, the reaction temperature is another important parameter that can greatly affect the final morphology and structure of the products in hydrothermal processes. To investigate the effect of the reaction temperature on the formation of Zn_2SiO_4 microspheres, experiments were carried out under different hydrothermal temperatures while keeping other conditions constant. The corresponding XRD pattern in Figure 6 showed that no zinc silicate was acquired at the low temperature of 120 ^{o}C, all of the reflections could be readily indexed to ZnO, suggesting that the resultant ZnO did not react with SiO_2 at lower temperature. The FESEM image showed the sample was a coexistence of irregular nanosheets and particles (Figure 7a). When the reaction temperature was in the range of 140–160 ^{o}C, pure $Zn_4Si_2O_7(OH)_2 \cdot H_2O$ bulk materials were obtained (Figure 7b

and c). Therefore, it can be assumed that higher reaction temperature can facilitate the formation of $Zn_4Si_2O_7(OH)_2 \cdot H_2O$. When the reaction temperature increased above 180 ^{o}C, some reflections from the Zn_2SiO_4 phase appeared, which indicated that the rhombohedral Zn_2SiO_4 crystalline phase started to form and the resulting sample was a mixture of $Zn_4Si_2O_7(OH)_2 \cdot H_2O$ and Zn_2SiO_4. Furthermore, the FESEM image (Figure 7d) confirmed that the bulk materials began to split into nanorods and nanoparticles. It can be concluded that $Zn_4Si_2O_7(OH)_2 \cdot H_2O$ is stable below 180 ^{o}C through the hydrothermal treatment of 24 h. When the temperature was 200 ^{o}C, straw-bundle-like Zn_2SiO_4 nanostructures were obtained (Figure 7e and f). With an increase in the reaction temperature (220 °C), the self-assembled growth of more nanorods continued and finally formed Zn_2SiO_4 nanorod-assembled microspheres (Figure 2b). These results suggested that the relative higher temperature was favorable for the formation of the urchin-like Zn_2SiO_4 microspheres.
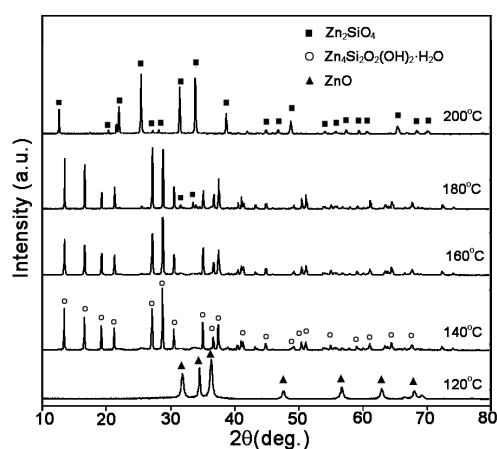

Fig. 6 XRD patterns of the products obtained at different hydrothermal temperatures.
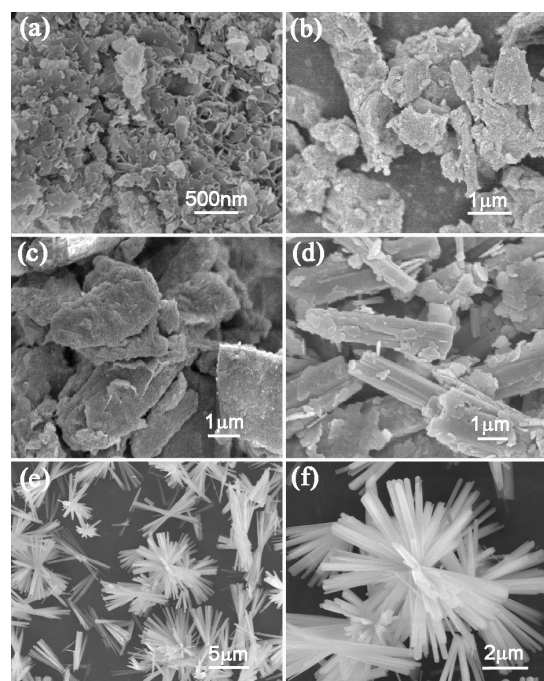

Fig. 7 FESEM images of the products obtained at different

hydrothermal temperatures: (a) 120, (b) 140, (c) 160, (d) 180, and (e), (f) 200 °C.

On the basis of above observations, the formation mechanism of the urchin-like Zn_2SiO_4 microspheres was proposed as follows. In the initial stage, ZnO nanostructures were formed through the reaction of $Zn(NO_3)_2$ and NaOH under the hydrothermal condition. The resulted ZnO then reacted with amorphous SiO_2 to form $Zn_4Si_2O_7(OH)_2 \cdot H_2O$. With the reaction processing, "a splitting process" occurs in which the $Zn_4Si_2O_7(OH)_2 \cdot H_2O$ bulk materials gradually splitted into Zn_2SiO_4 nanorods and nanoparticles, accompanied by a phase transformation from $Zn_4Si_2O_7(OH)_2 \cdot H_2O$ to Zn_2SiO_4. This process is driven by the H_2O molecular deintercalating from the interlayer spaces of $Zn_4Si_2O_7(OH)_2 \cdot H_2O$. It can be concluded that the $Zn_4Si_2O_7(OH)_2 \cdot H_2O$ is the intermediate phase of the hydrothermal procedure, and this result is consistent with previous studies.[33] As the reaction proceeded further, the Zn_2SiO_4 nanoparticles vanished and the longer nanorods formed. This process is in accordance with the well-known "Ostwald ripening mechanism".[34–36] At the same time, the OH^- adsorbed on the surface of the Zn_2SiO_4 nanorods would direct the self-assembly of nanorods by molecular interaction into urchin-like microspheres. Similar self-assembly process was observed in the preparation of $NiCo_2O_4$ and TiO_2 urchin-like microspheres.[2,37]
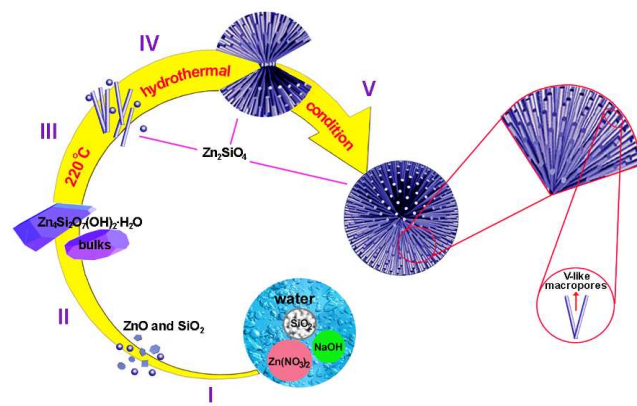

Fig. 8 Schematic illustration of the formation process of the Zn_2SiO_4 urchin-like microspheres. (I) formation of ZnO; (II) formation of $Zn_4Si_2O_7(OH)_2 \cdot H_2O$ bulk materials; (III) $Zn_4Si_2O_7(OH)_2 \cdot H_2O$ bulk materials split into Zn_2SiO_4 nanorods and nanoparticles; (IV) self-assembly of Zn_2SiO_4 nanorods; (V) formation of Zn_2SiO_4 urchin-like microspheres.

To investigate the application of the as-prepared Zn_2SiO_4 urchin-like microspheres in LIBs, the products were configured as electrodes to evaluate their electrochemical properties. Figure 9a displayed the charge-discharge curves of the Zn_2SiO_4 urchin-like microspheres in the initial three cycles in the voltage range of 0.02–2.5 V at a current density of 50 mA g^{-1}. As shown in Figure 9a, there was a wide, steady discharging plateau at 0.5V (vs Li^+/Li) in the first cycle, followed by a gradual voltage decrease. The discharge and charge capacities of the first cycle were 926 and 532 mAh g^{-1}, respectively, with a low initial Coulombic efficiency of 57.5 %. For the second discharge, the potential plateau shifted upward to near 1.0 V (vs Li^+/Li) with a more

sloping profile accompanied by a capacity loss. The discharge and charge capacities decreased to 528 and 515 mAh g^{-1}, respectively, resulting in an increased Coulombic efficiency of 97.5 %. Moreover, the Coulombic efficiency remained at ~ 97 % in the following cycles (Figure 9c). According to the results presented above, the urchin-like Zn_2SiO_4 microsphere electrode showed high initial discharge capacity and large irreversible capacity loss in the first cycle, which as partially contributed to the severe side reaction of the larger surface area with the electrolyte and the formation of a solid electrolyte interphase (SEI) film.[38,39] For comparison purposes, we also evaluated the electrochemical performance of the Zn_2SiO_4 bulk materials obtained from solid-state reaction (Figure S1). It can be seen that the initial discharge and charge capacities were 816 and 361 mAh g^{-1}, respectively, with a coulombic efficiency of 44.2 % (Figure 9b). In the second cycle, the discharge and charge capacities reached 344 and 328 mAh g^{-1} with a coulombic efficiency of about 95.3 %. A comparison of the cycling performance between the Zn_2SiO_4 urchin-like microsphere and Zn_2SiO_4 bulk materials was carried out, which was shown in Figure 9c. After 20 cycles, the retained reversible capacity of the Zn_2SiO_4 microsphere was 413 mAh g^{-1}, at a current density of 50 mA g^{-1}, while the Zn_2SiO_4 bulk materials retained only 190 mAh g^{-1}. In our previous work, the electrochemical properties of Zn_2SiO_4 nanorods and mesorods have also been studied. The results showed Zn_2SiO_4 nanorods and mesorods could retain the reversible capacities of 388 mAh g^{-1} and 311 mAh g^{-1}, respectively, after 20 cycles at a current of 50 mAg^{-1}. Therefore, the as-prepared urchin-like Zn_2SiO_4 microsphere showed much better discharge capacity and improved cycle stability as an anode material for LIBs compared to the Zn_2SiO_4 nanorods, mesorods and bulk materials.
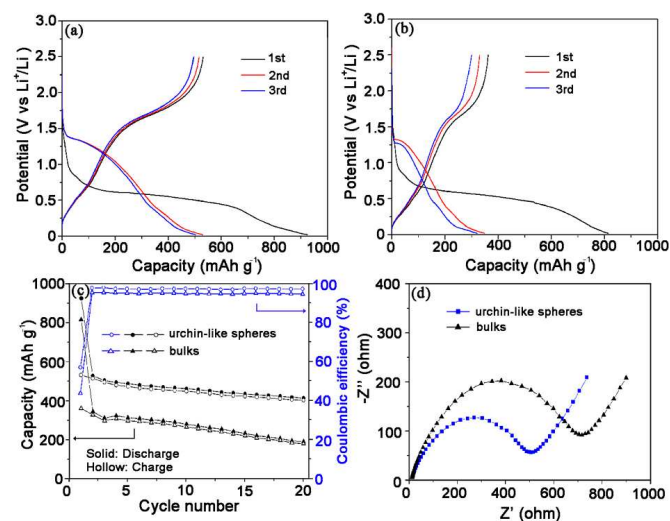

Fig. 9 Discharge/charge profiles of the as-prepared Zn_2SiO_4 (a) urchin-like microspheres and (b) bulk materials for the first three cycles in the voltage range of 0.02−2.5 V at the current density of 50 mA g^{-1}. (c) The discharge/charge capacity and Coulombic efficiency versus cycle numbers, and (d) Nyquist plots for Zn_2SiO_4 urchin-like microspheres and bulk materials.

To provide a deeper insight into the effect of morphology on the electrochemical performance of Zn_2SiO_4, electrochemical

impedance spectroscopy (EIS) measurements of the Zn_2SiO_4 urchin-like microspheres and bulk materials were carried out and shown in Figure 9d. The spectra of the two electrodes had a similar shape with one depressed semicircle in the high- and medium-frequency regions and an inclined line in the low-frequency region. The semicircle can be assigned to the combination of Li^+ migration resistance through the SEI film and the charge-transfer resistance at the electrode surface, and the linear portion can be assigned to the solid-state diffusion resistance of lithium ions within the host. Apparently, the semicircle diameter of the Zn_2SiO_4 urchin-like microspheres was much smaller than that of Zn_2SiO_4 bulk materials, indicating that Zn_2SiO_4 urchin-like microspheres had much lower SEI resistance and charge-transfer resistance. Therefore, the unique hierarchical architecture was beneficial for enhancing the reaction kinetics, thus leading to higher reversible capacity and better cyclability.

To identify the lithiation mechanism of the Zn_2SiO_4 urchin-like microspheres, cyclic voltammogram (CV) was carried out in the voltage range of 0.01−3 V. Figure 10 represented the first three CV scans at a scanning rate of 0.2 mV s^{-1}. On the basis of the lithium storage mechanism of ZnO and SiO_2,[40,41] we proposed that the lithium insertion process on the as-prepared Zn_2SiO_4 urchin-like microspheres is as follows [Eqs. (1)−(3)]:
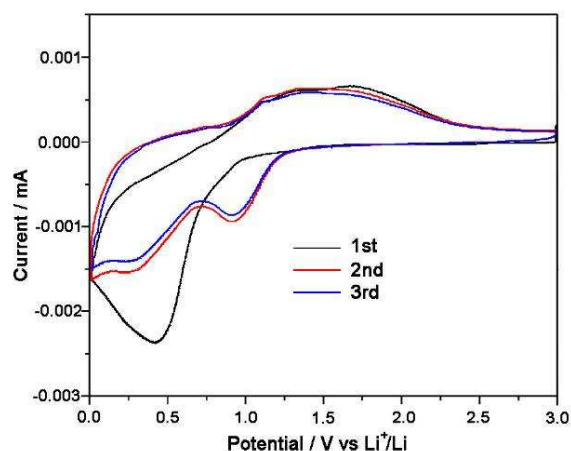
$$Zn_2SiO_4 + 4Li^+ + 4e \rightarrow 2Zn + SiO_2 + 2Li_2O \qquad (1)$$
$$Zn + xLi^+ + xe^- \leftrightarrow Li_xZn \quad (0 \leq x \leq 1) \qquad (2)$$
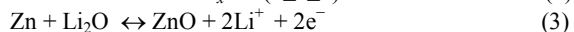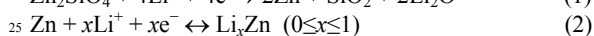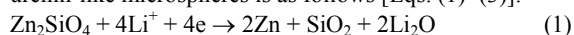$$Zn + Li_2O \leftrightarrow ZnO + 2Li^+ + 2e^- \qquad (3)$$

Fig. 10 The first three CV scans of the as-prepared Zn_2SiO_4 urchin-like microspheres.

The first cathodic scan for the Zn_2SiO_4 urchin-like microsphere electrode exhibits an irreversible reduction peak, which is large, broad and centered at 0.42 V. This peak is related to the first electrochemical process of Zn_2SiO_4, including the reduction of Zn_2SiO_4 to Zn and SiO_2 [Eq. (1)], the alloying reaction [Eqs. (2)], the oxidation of Zn to ZnO [Eqs. (3)], and the formation of the solid electrolyte interface (SEI) layer. The potentials of these electrochemical reactions are very close, so it shows only a strong reduction peak. In the subsequent anodic scan, the curve exhibits two broad peaks (1.3V and 1.7V), which can be ascribed to the dealloying process of Li–Zn alloy and the reduction of ZnO to Zn. In the second and subsequent cycles, two cathodic peaks are observed at around 0.28 and 0.91 V (vs Li^+/Li), which correspond to the reversible reactions of whole process [Eqs. (2) and (3)].

From the second cycle onwards, the CV curves are mostly overlapped, indicating the good reversibility of the electrochemical reactions.

According to the results presented above, the as-prepared Zn_2SiO_4 urchin-like microspheres exhibited superior electrochemical performances in terms of coulombic efficiency, specific capacity, and cycling performance, which is of great significance for LIBs. We believe the better electrochemical performances of the Zn_2SiO_4 urchin-like microspheres should be reasonably ascribed to their hierarchical porosity, good electronic pathways, and ordered microstructure. As shown in Figure 8, the Zn_2SiO_4 urchin-like microspheres are built up with many nanosized rods, which increases its electroactive surface and still maintains an ordered structure and rich ''V-type'' porous structure for ion transportation.[42,43] Furthermore, the diameter of the nanorods is much smaller than the corresponding bulk materials, which offer short solid-state diffusion length for Li insertion from surface to core of active materials, thus leading to a higher Li^+ diffusion rate and faster electronic kinetics, as demonstrated in a variety of 1D nanostructured electrodes.[44,45] In addition, the 3D hierarchical nanostructures could effectively accommodate the drastic volume changes during the lithium insertion/removal process, provide a larger electrode/electrolyte contact area and decrease the polarization of the electrode during the discharge–charge cycles, thereby increasing the discharge capacity.[14,46] As the capacity loss in metal oxide-type electrodes is associated with a large volume expansion that leads to particle pulverization and agglomeration during the cycles, the hierarchical nanostructures could possibly tolerate such changes better than the bulk materials.[44–46] Although the capacity retention rate of Zn_2SiO_4 urchin-like microspheres is lower than that of state-of-the-art electrode materials, with respect to the facile preparation and high yield of the product, the present Zn_2SiO_4 urchin-like microspheres demonstrate potential applications as anode materials for LIBs. As a new anode material, a detailed lithium storage process is unclear. Further research on the Li^+ intercalation and deintercalation process into the Zn_2SiO_4 urchin-like nanostructures is underway in our group to facilitate the application of Zn_2SiO_4 as an anode material as early as possible.

4. Conclusions

In summary, urchin-like Zn_2SiO_4 microspheres were successfully prepared by a simple and convenient hydrothermal method. The unique morphology and structural feature of Zn_2SiO_4 were significantly influenced by the reaction times, reaction temperatures, and pH values. According to comparative experimental results, a splitting and self-assembly process was proposed to elucidate the formation of the urchin-like microstructure. Electrochemical evaluation revealed that the Zn_2SiO_4 urchin-like microspheres exhibited higher discharge capacity and better cyclability than the Zn_2SiO_4 bulk materials. The reversible capacity of 413 mAh g^{-1} was delivered after 20 cycles at a current density of 50 mA g^{-1}, with coulomibic efficiency of about 97 %. The present work will greatly expand the range of anode choices and could assist long-term endeavors in developing high capacity anode materials for LIBs. Furthermore, the Zn_2SiO_4 nanostructure may also find potential

applications in other fields, such as catalysis, semiconductor, water purification, and so on.

Notes and references

[a] *College of Chemical Engineering, Shijiazhuang University, Hebei Province, Shijiazhuang, 050035, China. Tel: +86-311-66617326; E-mail: zsyedu@hotmail.com*
[b] *School of Materials Science and Engineering, Nanyang Technological University, Singapore, 639798, Singapore. Tel: +65-68725563; E-mail: sjpeng@ntu.edu.sg*
† Electronic Supplementary Information (ESI) available: FESEM image and XRD pattern of the Zn_2SiO_4 bulk materials. See DOI: 10.1039/b000000x/

1   B. Wang, H. B. Wu, L. Yu, R. Xu, T. T. Lim and X. W. Lou, *Adv. Mater.*, 2012, **24**, 1111.

2   Q. F. Wang, B. Liu, X. F. Wang, S. H. Ran, L. M. Wang, D. Chen and G. Z. Shen, *J. Mater. Chem.*, 2012, **22**, 21647.

3   J. Elias, C. Lévy-Clément, M. Bechelany, J. Michler, G. Y. Wang and Z. Wang, L. Philippe, *Adv. Mater.*, 2010, **22**, 1607.

4   L. P. Zhu, H. M. Xiao, X. M. Liu and S. Y. Fu, *J. Mater. Chem.*, 2006, **16**, 1794.

5   S. J. Peng, L. L. Li, P. N. Zhu, Y. Z. Wu, M. Srinivasan, S. G. Mhaisalkar, S. Ramakrishna and Q. Y. Yan, *Chem. Asian J.*, 2013, **8**, 258.

6   S. J. Peng, L. L. Li, H. T. Tan, Y. Z. Wu, R. Cai, H. Yu, X. Huang, P. N. Zhu, S. Ramakrishna, M. Srinivasan and Q. Y. Yan, *J. Mater. Chem. A*, 2013, **1**, 7630.

7   S. L. Chou, J. Z. Wang, H. K. Liu and S. X. Dou, *J. Phys. Chem. C*, 2011, **115**, 16220.

8   L. F. Xiao, Y. Q. Zhao, J. Yin and L. Z. Zhang, *Chem. Eur. J.*, 2009, **15**, 9442.

9   L. Zhou, D. Y. Zhao and X. W. Lou, *Adv. Mater.*, 2012, **24**, 745.

10 J. X. Zhu, Z. Y. Yin, H. Li, H. T. Tan, C. L. Chow, H. Zhang, H. H. Hng, J. Ma and Q. Y. Yan, *Small*, 2011, **7**, 3458.

11 X. H. Rui, J. X. Zhu, D. Sim, C. Xu, Y. Zeng, H. H. Hng, T. M. Lim and Q. Y. Yan, *Nanoscale*, 2011, **3**, 4752.

12 H. Kim, B. Han, J. Choo and J. Cho, *Angew. Chem. Int. Ed.* 2008, **47**, 10151.

13 X. H. Rui, H. T. Tan, D. H. Sim, W. L. Liu, C. Xu, H. H. Hng, R. Yazami, T. M. Lim and Q. Y. Yan, *J. Power Sources*, 2013, **222**, 97.

14 W. X. Zhang, M. Li, Q. Wang, G. D. Chen, M. Kong, Z. H. Yang and S. Mann, *Adv. Funct. Mater.*, 2011, **21**, 3516.

15 J. Z. Zhao, Z. L. Tao, J. Liang and J. Chen, *Cryst. Growth Des.*, 2008, **8**, 2799.

16 L. Hu, H. Zhong, X. R. Zheng, Y. M. Huang, P. Zhang and Q. W. Chen, *Sci. Rep.*, 2012, **2**, 986.

17 S. Y. Zhang, X. Xiao, M. Lu and Z. Q. Li, *J. Mater. Sci.* 2013, **48**, 3679.

18 C. Bartohu, J. Benoit, P. Benalloul and A. Morell, *J. Electrochem. Soc.*, 1994, **141**, 524.

19 X. F. Wang, H. T. Huang, B. Liu, B. Liang, C. Zhang, Q. Ji, D. Chen and G. Z. Shen, *J. Mater. Chem.*, 2012, **22**, 5330.

20 Y. P. Guo, H. Ohsato and K. I. Kakimoto, *J. Eur. Ceram. Soc.*, 2006, **26**, 1827.

21 J. S. An, J. H. Noh, I. S. Cho, H. S. Roh, J. Y. Kim, H. S. Han and K. S. Hong, *J. Phys. Chem. C*, 2010, **114**, 10330.

22 J. X. Wan, X. Y. Chen, Z. H. Wang, L. Mu and Y. T. Qian, *J. Cryst. Growth*, 2005, **280**, 239.

23 L. W. Yang, X. L. Wu, G. S. Huang, T. Qiu, Y. M. Yang and G. G. Siu, *Appl. Phys. A*, 2005, 81, 929.

24 H. F. Wang, Y. Q. Ma, G. S. Yi and D. P. Chen, *Mater. Chem. Phys.*, 2003, 82, 414.

25 X. F. Wang, H. T. Huang, B. Liu, B. Liang, C. Zhang, Q. Ji, D. Chen and G. Z. Shen, *J. Mater. Chem.*, 2012, **22**, 5330.

26 Y. Jiao, Y. Liu, F. Y. Qu, X. Wu. *CrystEngComm*, 2014, **16**, 575.

27 F. Zhang, J. Li, J. Shan, L. Xu and D. Y. Zhao, *Chem. Eur. J.*, 2009, **15**, 11010.

28 C. H. An, Y. J. Wang, Y. N. Huang, Y. N. Xu, C. C. Xu, L. F. Jiao, H. T. Yuan, *CrystEngComm*, 2014, **16**, 385.

29 K. -H. Klaska, J. C. Eck and D. Pohl, *Acta Cryst.*, 1978, **B34**, 3324.

30 H. Chang, H. D. Park, K. S. Sohn and J. D. Lee, *J. Korean Phys. Soc.*, 1999, **34**, 545.

31 S. Y. Zhang, M. Lu, Y. Li, F. Sun, J. C. Yang and S. L. Wang, *Mater. Lett.*, 2013, **100**, 89.

32 W. Stöber and A. Fink, *J. Colloid Interface Sci.*, 1968, **26**, 62.

33 H. F. Wang, Y. Q. Ma, G. S. Yi and D. P. Chen, *Mater. Chem. Phys.*, 2003, **82**, 414.

34 Z. A. Peng and X. G. Peng, *J. Am. Chem. Soc.*, 2001, **123**, 1389.

35 H. Ma, S. Y. Zhang, W. Q. Ji, Z. L. Tao and J. Chen, *J. Am. Chem. Soc.*, 2008, **130**, 5361.

36 S. Y. Zhang, L. J. Ci and H. R. Liu, *J. Phys. Chem. C*, 2009, **113**, 8624.

37 W. H. Wang, W. Z. Wang and H. X. Xu, *Chin. Phys. Lett.*, 2011, **28**, 078103.

38 D. Aurbach, B. Markovsky, M. D. Levi, E. Levi, A. Schechter, M. Moshkovich and Y. Cohen, *J. Power Sources*, 1999, **81–82**, 95.

39 A. Rong, X. P. Gao, G. R. Li, T. Y. Yan, H. Y. Zhu, J. Q. Qu and D. Y. Song, *J. Phys. Chem. B*, 2006, **110**, 14754.

40 H. Usui, T. Kono and H. Sakaguchi, *Int. J. Electrochem. Sci.*, 2012, **7**, 4322.

41 X. F. Li, A. Dhanabalan, X. B. Meng, L. Gu, X. L. Sun and C. L. Wang, *Microporous Mesoporous Mater.*, 2012, **151**, 488.

42 C. Z. Yuan, X. G. Zhang, L. R. Hou, L. F. Shen, D. K. Li, F. Zhang, C. G. Fan and J. M. Li, *J. Mater. Chem.*, 2010, **20**, 10809.

43 Y. G. Wang, H. Q. Li and Y. Y. Xia, *Adv. Mater.*, 2006, **18**, 2619.

44 S. Y. Zhang, W. Y. Li, C. S. Li and J. Chen, *J. Phys. Chem. B*, 2006, **110**, 24855.

45 W. Y. Li, F. Y. Cheng, Z. L. Tao and J. Chen, *J. Phys. Chem. B*, 2006, **110**, 119.

46 H. Kim, B. Han, J. Choo and J. Cho, *Angew. Chem. Int. Ed.*, 2008, **47**, 10151.

Graphical Abstract
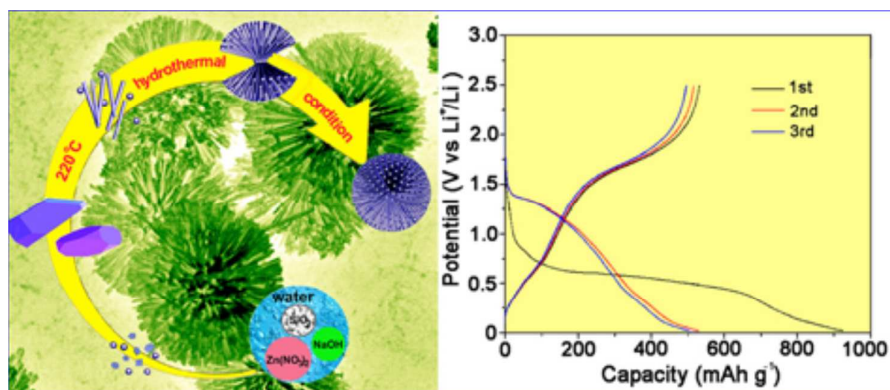
Three-dimensional Zn_2SiO_4 urchin-like microspheres have been fabricated by a one-step hydrothermal procedure.